

Free Energy Calculations in Electroactive Self-Assembled Monolayers (SAMs): Impact of the Chain Length on the Redox Reaction

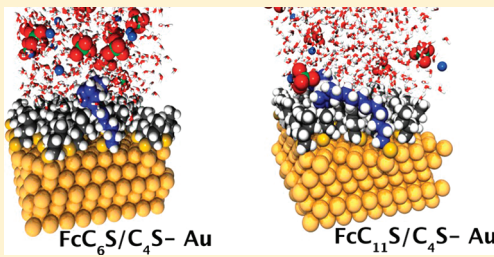
Gaëlle Filippini,[†] Yael Israeli,[‡] Florent Goujon,[†] Benoit Limoges,[§] Christine Bonal,^{*,†} and Patrice Malfreyt[†]

[†]Laboratoire de Thermodynamique et Interactions Moléculaires, UMR CNRS 6272, Université Blaise Pascal, 63177 Aubière Cedex, France

[‡]Laboratoire de Photochimie Moléculaire et Macromoléculaire, UMR CNRS 6505, Université Blaise Pascal, 63177 Aubière Cedex, France

[§]Laboratoire d'Electrochimie Moléculaire, UMR CNRS 7591, Université Paris Diderot, 15 rue Jean-Antoine de Baïf, 75205 Paris Cedex 13, France

ABSTRACT: The free energy approach is used to study the effect of the relative chain length of the two constituents of electroactive self-assembled monolayers (SAMs) on gold. In this study, the ferrocene groups are exposed to the electrolyte solution. This situation is achieved by using shorter diluent alkanethiol chains. To this end, the mixed monolayers formed by the self-assembly of 11-ferrocenylundecanethiol and butanethiol $\text{FcC}_{11}\text{S}/\text{C}_4\text{S}$ and of 6-ferrocenylhexanethiol and butanethiol $\text{FcC}_6\text{S}/\text{C}_4\text{S}$ onto a gold surface are studied. Calculation of enthalpy and entropy differences are also performed using molecular simulations. Additionally, the electrochemical signatures of these systems are determined to allow a direct comparison with our calculations. The thermodynamic properties are discussed in terms of enthalpy and entropy changes. Two effects account for the thermodynamic behavior. The first one involves the ion pairing between the ferrocenium group and the perchlorate anion. The second one concerns the desolvation of the first hydration shell of the anions. Finally, this work is also completed with a microscopic description associated with an energy characterization of these SAMs as a function of the surface coverage under conditions close to experiments.



INTRODUCTION

Self-assembled monolayers (SAMs) have attracted considerable attention because they provide a mean to control interfacial properties for different applications in chemical, electronic, and biotechnological fields.^{1–7} The use of alkanethiols which contain terminal redox-active groups opens up the possibility of obtaining more information about SAM structure and investigating the mechanisms of electron transfer from the molecular layer to the electrode within a well-defined chemical environment.^{8–12} In fact, it is well-known that the kinetics and thermodynamics of interfacial redox reactions are strongly affected by the nature of the medium in which they occur. A promising strategy for studying local medium effects on electrode reactions is to form a two-component self-assembled monolayer film in which a redox-active moiety is included. Ferrocene (Fc) is an ideal choice for incorporation into the alkylthiolate SAMs. It has the advantage of having relatively straightforward electrochemistry in the sense that every surface-tethered ferrocene can be reversibly interrogated by electrochemistry. Consequently, the ferrocene-terminated SAMs are extensively used to study the effects of the nature of the terminal group and the solvent, of the relative concentration of each component in the coating solution, and of the relative chain length of the two constituents linked to the surface.

As part of our interest in this area, we have been researching approaches to study the fundamental chemistry and physical

interactions that control the formation, structure, and the reactivity of these chemically modified surfaces. From the electrochemical data it is possible to assess to the packing and the degree of order of the monolayers. The electrochemical characteristics of these mixed SAMs clearly indicate that both the shape and the peak potential of the redox waves are strongly affected by physical interactions such as those between the ferrocenylalkanethiolates in the SAMs^{8,11} or between the ferrocene groups and the electrolyte ions.^{13,14} The effect of the relative chain lengths of the coadsorbates is also an important issue which needs to be addressed in many applications. In fact, by changing the length of the carbon chain, one can deliberately control the order of the system. Then, it has been established that longer alkyl chains preferentially adsorb leading to a more ordered structure compared to their equivalent shorter ones. This is due to van der Waals interactions between the alkyl chains. Consequently, most of the studies have been performed on gold electrodes with longer alkyl chains.^{13,15–23}

Molecular dynamics (MD) simulations have shown to be highly successful in capturing both the structural and the energetic properties of SAMs.^{24–28} Actually, molecular dynamics simulations have been performed in conditions close to the

Received: May 18, 2011

Revised: August 24, 2011

Published: August 25, 2011

electrochemical experiments²⁷ to obtain a better understanding into these electrochemical systems.²⁷ For this purpose, a supporting electrolyte was added, and the electron transfer process was modeled through simulations of ferrocene in both its neutral and oxidized forms. More recently, we have demonstrated that molecular simulation can also be used to obtain quantitative information about electrochemical experiments.²⁸ Indeed, the free energy perturbation methods are able to reproduce the change in the redox potential in electroactive SAMs as the environment of the ferrocene moiety is modified. To this end, we studied two systems: a binary SAM formed by ferrocenylhexanethiol and coadsorbed dodecanethiol ($\text{FcC}_6\text{S}/\text{C}_{12}\text{S}$ –Au), and another binary SAM composed of ferrocenylhexanethiol and coadsorbed butanethiol ($\text{FcC}_6\text{S}/\text{C}_4\text{S}$ –Au). The replacement of the coadsorbed butanethiolate by dodecanethiolate chains induced a positive shift of the redox potential. This shift was due to the partial immersion of the redox center in the hydrocarbon layer. This environment stabilized ferrocene to a greater extent than for ferricinium. The magnitude of the shift was successfully reproduced by our free energy calculations.

In the present work, we have re-examined the question of the effect of the relative chain length of the two constituents linked to the surface. However, we have decided to consider here the unusual case where the ferrocene groups are exposed to the electrolyte solution. This situation can be achieved by using shorter diluent alkanethiol chains. The investigated monolayer structure is $\text{FcC}_{11}\text{S}/\text{C}_4\text{S}$ –Au. The results are compared with those of $\text{FcC}_6\text{S}/\text{C}_4\text{S}$ –Au monolayer that are more commonly studied. First, the free energy formalism is used to predict the change in the simulated redox properties of these two systems. Calculations of enthalpy and entropy differences using molecular simulations are also performed. Additionally, the electrochemical signatures of these systems are determined to obtain direct comparison with our calculations. This allows us to associate the free energy calculations to complement the electrochemical results at both molecular and energetic levels. This work is also completed with a microscopic description associated with an energy characterization of these SAMs as a function of the surface coverage using conditions close to experiments. For this purpose, the corresponding supporting electrolyte is added, and the redox process is modeled through molecular simulation of Fc in both its neutral and oxidized form.

The outline of this work is as follows. In the section concerning the experimental methods, we give the details of the computational procedures and of the electrochemical measurements. In the next section, we present the results obtained by the free energy perturbation approach and by cyclic voltammetry. Later in the section, we discuss the structural and energetic properties deduced from MD simulations. Finally, in the last section we draw the main conclusions from this work.

■ EXPERIMENTAL SECTION

Molecular Dynamics Simulation. The system consists of five layers of a Au(111) surface grafted with n - FcC_{11}S or n - FcC_6S ferrocenylalkylthiolate molecules. Dilute n - C_4S alkylthiolate chains are grafted onto the surface at every available grafting point. The surface is in contact with a water phase containing NaClO_4 1 M as a supporting electrolyte. We used the all-atom (AA) version of the Cornell force field AMBER²⁹ for grafted molecules. The Au parameters were taken from the work of

Ayappa and co-workers.³⁰ The ferrocene part was modeled using the parameters described by Canongia et al.³¹ The general potential function is of the form

$$U = \sum_{\text{bonds}} k_b(r - r_o)^2 + \sum_{\text{angles}} k_\theta(\theta - \theta_o)^2 + \sum_{\text{dihedrals}} k_\phi[1 + \cos(l\phi + \delta)] \\ + \sum_{i=1}^{N-1} \sum_{j=i+1}^N \left\{ 4\varepsilon_{ij} \left[\left(\frac{\sigma_{ij}}{r_{ij}} \right)^{12} - \left(\frac{\sigma_{ij}}{r_{ij}} \right)^6 \right] + \sum_l^{\infty} \frac{q_i q_j}{|r_{ij} + nL|} \right\} \quad (1)$$

where k_b , k_θ , and k_ϕ are the force constants for deformation of bonds, angles, and dihedrals, respectively. The equilibrium values of bond distances and valence angles correspond to r_o and θ_o , respectively. In the dihedral angle term, l is the periodicity, and δ is the phase factor. The C–H covalent bonds were kept of fixed length by using the SHAKE algorithm.³² The intermolecular and intramolecular interactions consist of a van der Waals repulsion–dispersion term calculated using the Lennard–Jones (6–12) potential, represented by the penultimate term in eq 1. In the AMBER force field, the nonbonded interactions between atoms separated by exactly three bonds (1–4 van der Waals interactions) are reduced by a factor of 0.5.²⁹ The Lennard–Jones potential parameters for the interactions between unlike atoms were calculated by using the Lorentz–Berthelot mixing rules (geometric and arithmetic rules for ε_{ij} and σ_{ij} parameters, respectively). The water molecules were represented with the TIP4P/2005 model.³³ As the system is nonperiodic in the direction normal to the surface (z -axis), the simulation cell is closed by an additional gold layer. The distance between the two inner surfaces was chosen to be 50 Å, which is large enough for the water molecules in the middle of the cell to have a bulk behavior.³⁴ The simulation cell was then extended both ways along z -axis with vacuum to prevent electrostatic interactions between neighboring cells evaluated using the Ewald summation. A supporting electrolyte NaClO_4 is added in the water phase. The Na^+ and ClO_4^- ions are represented with the model described by Wu et al.³⁵

Long-Range Coulombic Interaction. The last term in eq 1 corresponds to the electrostatic energy (U_{ele}) of the system. The electrostatic interactions are calculated with the smooth particle mesh Ewald (SPME) method.³⁶ For a neutral periodic system with orthogonal axis, the electrostatic potential U_{ele} is defined as

$$U_{\text{ele}} = U_{\text{R}} + U_{\text{K}} + U_{\text{self}} + U_{\text{excl}} + U_{\text{ch}} + U_{M_z} \quad (2)$$

$$U_{\text{R}} = \frac{1}{8\pi\varepsilon_o} \sum_i \sum_a \sum_{j \neq i} \sum_b q_{ia} q_{jb} \frac{\text{erfc}(\alpha r_{iajb})}{r_{iajb}} \quad (3)$$

where the sums are over all atoms a in molecule i and all atoms b in molecule j . r_{iajb} is the distance between the atoms a and b belonging to two different molecules i and j , and q_{ia} and q_{jb} represent the charges on atoms a and b , respectively. This term is pairwise-additive and short-ranged, and a spherical cutoff can be used with periodic boundary conditions. α is chosen so that only atom–atom pair interactions between different molecules in the central cell ($n = 0$) need to be considered. $\text{erf}(x)$ is the error function, whereas $\text{erfc}(x)$ is the complementary error function. Note that the overall charge of the simulation box must be zero.

The reciprocal space part U_K of the potential is expressed as

$$U_K = \frac{1}{2V\epsilon_0} \sum_{k \neq 0} \frac{1}{k^2} \exp\left(-\frac{k^2}{4\alpha^2}\right) \left| \sum_i \sum_a q_{ia} \exp(-ik \cdot r_{ia}) \right|^2 \quad (4)$$

where V is the simulation cell volume and r_{ia} is the Cartesian coordinate of site a in molecule i . The reciprocal lattice vector \mathbf{k} is defined as $\mathbf{k} = 2\pi(l/L_x \mathbf{u}, m/L_y \mathbf{v}, n/L_z \mathbf{w})$ where \mathbf{u} , \mathbf{v} , and \mathbf{w} are the reciprocal space basis vectors and l , m , and n take values of $0, \pm 1, \pm 2, \dots \pm \infty$. The reciprocal space sum is truncated at an ellipsoidal boundary at the vector $|\mathbf{k}|^{\max}$. This term includes all of the intramolecular interactions due to the bonded atoms.

The U_{excl} term is added to correct for the contributions due to intramolecular electrostatic interactions. It is expressed as

$$U_{\text{excl}} = -\frac{1}{8\pi\epsilon_0} \sum_i \sum_a \sum_{b \neq a} q_{ia} q_{ib} \frac{\text{erf}(\alpha r_{iab})}{r_{iab}} \quad (5)$$

where the sums are over atoms bonded to atoms a and b of the same molecule i through bonds, valence, and dihedral potentials.

A fourth correction U_{self} term is required to correct for the fact that the sum of Gaussian functions in the real space includes the interactions of each Gaussian with itself.

$$U_{\text{self}} = -\frac{\alpha}{4\pi r^{3/2} \epsilon_0} \sum_i \sum_a q_{ia}^2 \quad (6)$$

The U_{ch} term is the Fuchs correction³⁷ added to the Ewald sum to prevent the resulting background charge created in the case of an electrically non-neutral simulation cell.

$$U_{\text{ch}} = -\frac{1}{4\pi\epsilon_0} \frac{1}{V\alpha^2} \left(\sum_i^N q_i \right)^2 \quad (7)$$

A sixth term, U_{M_z} , is included to consider the supercell approximation³⁸ and is defined as

$$U_{M_z} = \frac{1}{2\epsilon_0 V} M_z^2 \quad (8)$$

where M_z is the net dipole moment of the simulation cell given by $\sum_{i=1}^N q_i \mathbf{r}_i$. This contribution is the correction term of Yeh and Berkowitz³⁸ which results from the plane-wise summation method proposed by Smith.³⁹ Adding this term to the total energy implies the use of a z -component force for each atom given by

$$F_{i,z} = -\frac{q_i}{\epsilon_0 V} M_z \quad (9)$$

The supercell approximation³⁸ consists of elongating the z -dimension of the simulation cell by placing an empty space of at least four times the space of the fluid-occupied region. The use of this approximation and the dipole correction allow to apply the conventional three-dimensional SPME technique to the calculation of the electrostatic interactions in a slab geometry.³⁴

Free Energy Calculations. The differences in Helmholtz free energies between states (0) and (1) of a same molecular system are calculated using the thermodynamic integration (TI) method. We showed previously that the TI and the finite difference thermodynamic integration (FDTI) methods give comparable results on our systems.²⁸

The perturbation process is performed between states (0) and (1) in the constant-NVT ensemble using a “double wide

sampling” over N_w intermediate contiguous windows defined by the coupling constant λ . The TI method expresses the change in Helmholtz free energy as the following integral

$$\Delta A_{\text{TI}} = \int_0^1 \left\langle \frac{\partial U(r, \lambda)}{\partial \lambda} \right\rangle \, d\lambda \quad (10)$$

where the derivative of $U(r, \lambda)$ with respect to λ can be calculated using a central finite difference technique between $U(r, \lambda + \delta\lambda)$ and $U(r, \lambda - \delta\lambda)$

$$\left\langle \frac{\partial U(r, \lambda)}{\partial \lambda} \right\rangle_{\lambda, \text{CD}} = \left\langle \frac{(U(r, \lambda + \delta\lambda) - U(r, \lambda - \delta\lambda))}{2\delta\lambda} \right\rangle_\lambda \quad (11)$$

$\delta\lambda$ is taken sufficiently small ($\delta\lambda = 0.0001$) to avoid hysteresis between calculations carried out from state λ to state $\lambda + \delta\lambda$ and from state λ to state $\lambda - \delta\lambda$. The integration over λ is carried out by a trapezoidal algorithm.

As shown previously,²⁸ the Helmholtz free energy change (ΔA) can be assimilated to Gibbs free energy change (ΔG) in specific thermodynamic conditions that are satisfied in the present calculations.

The entropy change ΔS calculated using TI approach⁴⁰ is given by

$$\Delta S = \frac{1}{kT^2} \int_0^1 \left[\left\langle U(r, \lambda) \right\rangle_\lambda \left\langle \frac{\partial U(r, \lambda)}{\partial \lambda} \right\rangle_\lambda - \left\langle \frac{\partial U(r, \lambda)}{\partial \lambda} \right\rangle_\lambda U(r, \lambda) \right] \, d\lambda \quad (12)$$

Simulation Details. The equations of motion were integrated using the Verlet leapfrog algorithm scheme at $T = 298$ K with a time step equal to 2 fs. The configurations were generated using the parallel version of the modified DL_POLY_MD package⁴¹ by using up to eight processors at a time. The parameters of the long-range electrostatics interactions evaluated by the SPME technique were calculated to satisfy a relative error of 10^{-6} . Simulations were run in the constant-NVT statistical ensemble using the Hoover thermostat⁴² with a coupling constant of 0.5 ps. Keeping the cell volume constant is useful for preserving a vacuum zone between periodic images along the z -axis. Two systems, A and B, were considered: system A corresponding to the $\text{FcC}_6\text{S}/\text{C}_4\text{S}-\text{Au}$ and system B corresponding to the $\text{FcC}_{11}\text{S}/\text{C}_4\text{S}-\text{Au}$.

Free energy calculations were performed using a perturbation process which consisted of the oxidation of the ferrocene moiety. In both A and B systems, the ferrocene charge was progressively increased from 0.0 ($\lambda = 0.0$) to 1.0 ($\lambda = 1.0$). The partial charges of the ferricinium group were calculated from the density functional theory (DFT)^{43,44} (B3LYP)⁴⁵⁻⁴⁷ with effective core potential (SD-DALL) Gaussian basis using the Gaussian 03 package⁴⁸ and the CHELPG⁴⁹ procedure as a grid-based method. The perturbation of the partial charges affects all of the atoms of the ferrocene group and the last three methylene groups of the alkyl chain bounded to ferrocene through bonds, valence, and dihedral angle potentials. These atoms are represented in Figure 1. The perturbation was carried over 11 contiguous states or windows defined by the coupling parameter λ . The atomic site charge q was calculated using a linear combination as

$$q_i(\lambda) = \lambda q_i(1) + (1 - \lambda) q_i(0) \quad (13)$$

where i represents the perturbed atomic site.

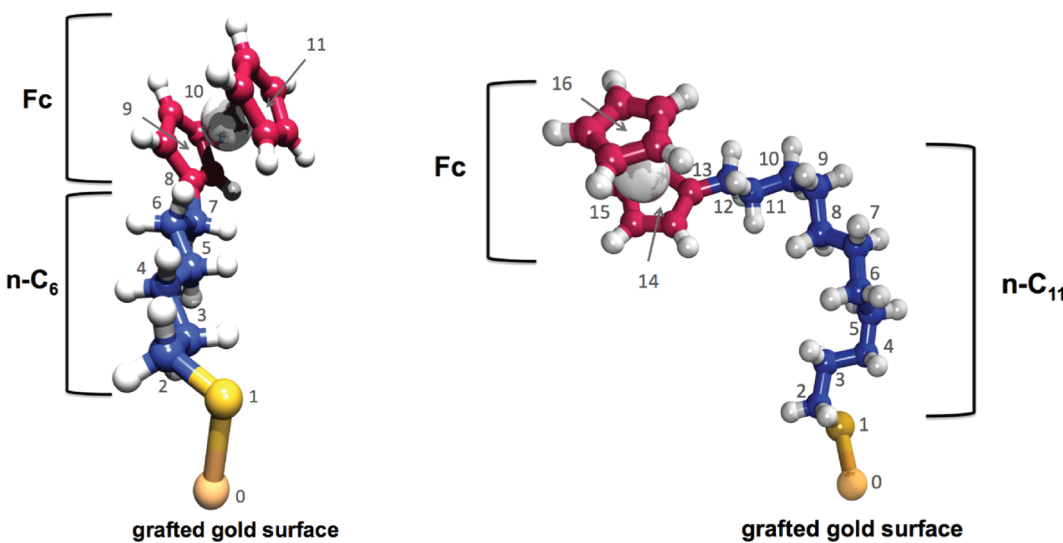


Figure 1. Scheme of the two ferrocenylalkanethiolate chains $\text{FcC}_6\text{S}-\text{Au}$ and $\text{FcC}_{11}\text{S}-\text{Au}$ used in this work with the atom numbering.

To reduce the size of the simulation cell and hence the computational cost of the simulations, only one ferrocenylalkylthiolate chain was perturbed at a time. As a consequence, free energy calculations were obtained from simulations of low grafting density monolayers ($2.5 \times 10^{-11} \text{ mol/cm}^2$). This value corresponds to about 5% ($\chi_{\text{Fc}}^{\text{Sur}} = 0.05$) of the theoretical maximum value ($4.5 \times 10^{-10} \text{ mol/cm}^2$) based on the assumption of hexagonal packing of the ferrocene moiety and by treating ferrocene as a sphere of diameter 6.6 \AA .⁵⁰ The simulation cell was constituted of a gold surface composed by five (111) layers of 9×10 FCC lattice so that the dimension of the simulation box along x and y axis were 25.9 \AA and 24.9 \AA , respectively. One ferrocenylhexanethiolate (FcC_6S) chain for system A or one ferrocenylundecanethiolate (FcC_{11}S) chain for system B was grafted onto the surface with an initial tilt angle $\theta = 30^\circ$. The remaining space was filled by grafting $27 \text{ C}_4\text{S}$ alkylthiolate using a minimal distance between grafting points corresponding to the experimental surface coverage of $1/3$. The water molecules and the cations and anions of the supporting electrolyte were randomly added to respect a concentration of 1 M for the electrolyte and an accurate bulk density for water. The size of the simulation cell along x and y axis implies the use of a cutoff radius of 12 \AA for the Lennard-Jones and the real space of the electrostatic interactions. The reciprocal space cutoff radius k_{\max} is fixed at 1.80 \AA^{-1} . A typical simulation run consisted of an equilibrium period of 500 ps and an additional acquisition phase of 400 ps . The total simulation for completing the perturbation calculation over 11 windows was about 10 ns .

To study the effect of the ferrocene surface coverage, additional system sizes were considered. Then, the system was extended along the x and y axis. The gold surface was composed by five layers of a 15×16 hexagonal lattice, so that the dimensions of the simulation box along the x and y axis were $43.2 \times 39.9 \text{ \AA}^2$. A number n_{AlkFc} of FcC_{11}S -chains was randomly grafted onto the surface with an initial tilt angle $\theta = 30^\circ$. The remaining space was filled by grafting C_4S -chains, using a minimal distance between grafting points corresponding to the experimental surface coverage of $1/3$. The number of alkylferrocene chains for the three systems simulated was chosen so that the surface grafting density is $\chi_{\text{Fc}}^{\text{Sur}} = 0.2$, $\chi_{\text{Fc}}^{\text{Sur}} = 0.4$, and $\chi_{\text{Fc}}^{\text{Sur}} = 1.0$,

Table 1. Summary of the Number of the Different Molecules in the Simulated Systems^a

system	$\chi_{\text{Fc}}^{\text{Sur}}$	n_{alkFc}	n_{alk}	$n_{\text{ClO}_4^-}$	n_{Na^+}	n_{water}	n_{atoms}
$\text{FcC}_{11}\text{S}/\text{C}_4\text{S}-\text{Au}$	0.2, neutral	10	58	42	42	2300	12264
	0.2, oxidized	10	58	42	32	2300	12264
	0.4, neutral	19	49	42	42	2250	12442
	1.0, neutral	48	0	16	16	890	7496
$\text{FcC}_6\text{S}/\text{C}_4\text{S}-\text{Au}$	0.2, neutral	10	58	42	42	2300	12114
	0.2, oxidized	10	58	42	32	2300	12114
	0.4, neutral	19	49	42	42	2300	12357
	1.0, neutral	48	0	31	31	1650	9906

^a n_{alk} and n_{AlkFc} are the number of grafted alkyl (C_4) and alkylferrocene (C_{11} or C_6) molecules, respectively. The number of water molecules n_{water} is adjusted so that the bulk density is respected. The overall zero charge of the system is respected by removing n_{Na^+} cations in the oxidized systems.

respectively. A fourth system was simulated at $\chi_{\text{Fc}}^{\text{Sur}} = 0.2$ with oxidized ferrocene headgroups. To neutralize the total charge of the simulation box, a sodium cation was removed from the system for each oxidized molecule. Concerning the system with alkylferrocene molecules only, the size of the surface was adjusted because the maximal surface coverage of ferrocene-terminated molecule is only $1/4$ due to the size of the ferrocene. Thus the surface of this system was composed by 12×16 unit cells, so that the dimensions of the simulation box along the x and y axis were $34.6 \times 39.9 \text{ \AA}^2$. The water and NaClO_4 molecules were randomly added in the remaining volume to respect a concentration of 1 M for the supporting electrolyte and an accurate bulk density for water. The same systems were simulated using FcC_6S molecules as the alkylferrocene grafted chains. The summary of the different numbers of each type of molecule used in these eight systems is reported in Table 1. For all of these systems, one simulation run consisted of an equilibrium period of 500 ps and an acquisition period of 1 ns .

Chemicals and Substrates. 11-Ferrocenylundecanethiol (FcC_{11}SH) and n -butanethiol (C_4SH) were obtained from Prochimia and Aldrich, respectively, and used as received. 6-Ferrocenylhexanethiol

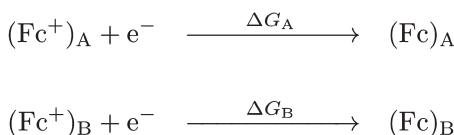


Figure 2. Redox reactions used to model the effect of the environment on the change in the redox properties of FcC_6S-C_4S-Au (system A represented by $(Fc)_A$) and $FcC_{11}S-C_4S-Au$ (system B represented by $(Fc)_B$) SAMs.

(FcC_6SH) was purchased from Aldrich and purified by flash chromatography (silica gel, 100:1 hexane/ethyl acetate). The structures were confirmed by 1H NMR spectroscopy. A deionized ultrapure water was used. All solvents and electrolytes were of commercial origin and were used as received.

The gold electrode (1 mm diameter) was sequentially mechanically polished to a mirror finish using diamond paste ($1\ \mu m$) and then alumina slurry ($0.3\ \mu m$) and finally sonicated for 5 min in ethanol. The electrode was electrochemically cleaned by a repetitive sweep from 0.3 to 1.5 V (vs SCE) in 0.1 M $HClO_4$ at a scan rate of 200 mV/s until a reproducible cyclic voltammogram was obtained. Finally, the electrode was submitted to a constant potential of 1.5 V for 5 min followed by a linear sweep from 1.5 to 0.3 V at 200 mV/s. The real surface area was estimated by recording cyclic voltammograms of reversible electrochemical markers such as ferricyanide.

Monolayers were formed at room temperature ($21\ ^\circ C$) by soaking gold substrates in a coating solution containing ferrocenylalkylthiolates and *n*-butanethiol (1.0 mM total thiol concentration) in absolute ethanol. The samples were removed from the coating solutions after a period of at least 24 h and washed with copious amounts of absolute ethanol followed by Milli-Q water. It was established that χ_{Fc}^{Sur} is consistently larger than χ_{Fc}^{Sol} for ferrocenylalkylthiolates SAMs diluted with shorter-chain length alkylthiols.^{14,51,52} Indeed, Row and Creager have obtained a $\chi_{Fc}^{Sur} = 0.2$ from a χ_{Fc}^{Sol} lower than 0.05 revealing a deviation from χ_{Fc}^{Sol} in FcC_6S-C_4S-Au monolayers.¹⁴ We therefore selected this ratio to prepare the SAMs at low Fc mole fraction.

Electrochemistry. Electrochemical measurements were carried out using a potentiostat/galvanostat model 273 PAR (Princeton Applied Research). All experiments were performed using a conventional three-electrode system with the gold disk electrode as the working electrode, a platinum electrode as the auxiliary electrode, and a saturated calomel electrode (SCE) as the reference electrode. To avoid potential chloride ion contamination, the reference electrode was separated from the electrochemical cell by a salt bridge containing saturated KNO_3 . The electrolyte solution was purged with N_2 gas prior to each measurement to minimize oxygen levels. The cyclic voltammograms were recorded in $HClO_4$ 1.0 M at $25^\circ C$. All the potential values were given with respect to SCE.

RESULTS AND DISCUSSION

We have shown in previous studies²⁸ that the redox reactions represented in Figure 2 allow us to compare the difference in the calculated free energies $\Delta\Delta G$ with the experimental results. This difference in the calculated free energies is obtained from $\Delta\Delta G = \Delta G_B - \Delta G_A$ where A refers to FcC_6S-C_4S-Au SAM and B refers to $FcC_{11}S-C_4S-Au$ SAM. Since we model the oxidative reactions, the computed free energies are of opposite sign

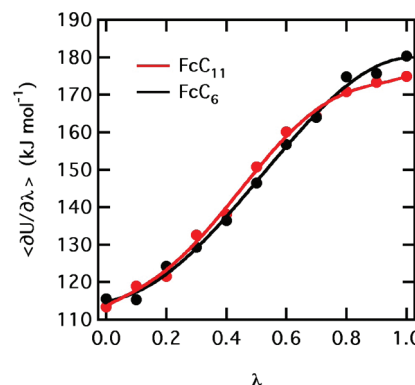


Figure 3. Average $\langle(\partial U(r,\lambda))/(\partial \lambda)\rangle_\lambda$ value as a function of λ in A and B.

Table 2. Differences in the $\Delta\Delta G_{redox}^{cal}$, the $T\Delta\Delta S_{redox}^{cal}$ (kJ/mol), and the $\Delta\Delta H_{redox}^{cal}$ (kJ/mol) Parameters Characterizing the Redox Reactions of A and B Calculated from Perturbation Methods

$-\Delta\Delta G_{redox}^{cal}$	$-\Delta\Delta H_{redox}^{cal}$	$-T\Delta\Delta S_{redox}^{cal}$
0.4	1.2	0.8

compared to experimental free energies that correspond to reductive processes.

Figure 3 shows the evolution of the total contribution $\langle(\partial U(r,\lambda))/(\partial \lambda)\rangle_\lambda$ with λ in A and B. We note that the evolution increases similarly for the two systems. The values of $\Delta\Delta G_{redox}^{cal}$ calculated using the numerical trapezoidal integration are given in Table 2. We also apply the operational expressions of eq 11 for the calculation of the entropy using the TI formalism.⁴⁰ The difference in the $T\Delta S$ is calculated from $T\Delta\Delta S = T\Delta S_B - T\Delta S_A$. The resulting $\Delta\Delta H = \Delta H_B - \Delta H_A$ is also reported in the same table. As concerns the Gibbs free energy, our result indicates a very small change in $\Delta\Delta G_{redox}^{cal}$. This redox property can be assimilated to $-nF\Delta E^{o'}$ where F is the Faraday's constant and n is the number of electrons involved in the electron transfer process ($n = 1$). $\Delta E^{o'}$ represents the difference of the redox potential (B – A). Consequently, free energy calculations predict a $\Delta E^{o'}$ of 4 mV. Such small values are difficult to measure from electrochemical experiments. It means that changing the ferrocenylalkanethiolate chain lengths in these systems does not induce a significant shift in redox potential under the conditions used here. This behavior is in sharp contrast to that observed previously.²⁸ Let us remember that we have demonstrated that, as the alkanethiol coadsorbate chain length increases, $\Delta E^{o'}$ shifts to more positive potentials, leading to significant differences between the Gibbs free energy of redox reaction.²⁸

We need now to check the prediction of the $\Delta E^{o'}$ by investigating the systems by experimental analyses. Cyclic voltammetry is used to obtain the electrochemical signature of tethered ferrocenes in binary SAMs. It allows the determination of the quantity of immobilized ferrocenes (Γ in mol/cm^2) by integration of the peak potential and the apparent formal redox potential $E^{o'}$, taken as the average of the anodic and cathodic peak potentials. The typical cyclic voltammograms of the mixed monolayers formed at low Fc mole fractions from the $FcC_{11}S-C_4S-Au$ monolayer and from the FcC_6S-C_4S-Au monolayer in 1.0 M $HClO_4$ electrolyte are represented in Figure 4. The

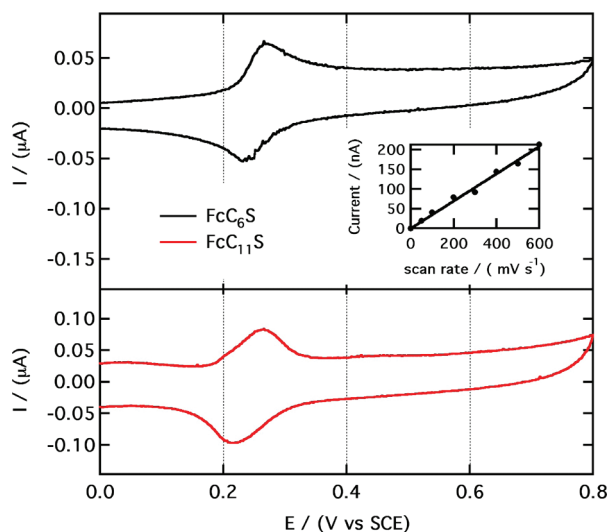


Figure 4. Cyclic voltammograms of SAMs in 1.0 M HClO_4 at 100 mV/s. The ferrocene coverage is $10^{-10} \text{ mol/cm}^2$ ($\chi_{\text{Fc}}^{\text{Sur}} = 0.2$) for the two monolayers. The inset shows the linear dependence of the peak currents on the scan rate for the anodic process of $\text{FcC}_6\text{S}/\text{C}_4\text{S}-\text{Au}$.

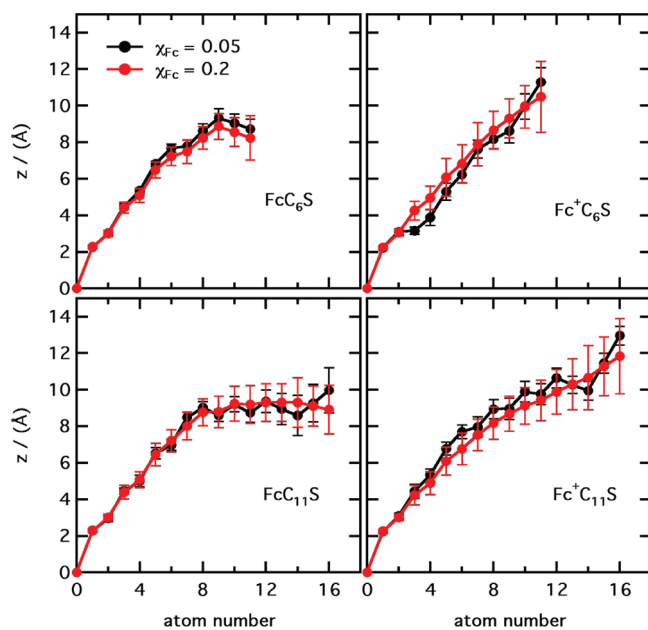


Figure 5. z position of all atoms of the ferrocenylalkylthiolate chains along the z -direction at $\chi_{\text{Fc}}^{\text{Sur}} = 0.05$ and $\chi_{\text{Fc}}^{\text{Sur}} = 0.2$ for the two studied systems before and after the oxidation of the ferrocene (see Figure 1 for the atom numbering).

electrode potential is scanned from -0.2 to 0.8 V/SCE. These mixed SAMs are stable and do not show variation in peak height or shape over numerous scans. The inset in Figure 4 is the relationship between peak currents and scan rate for the anodic process of $\text{FcC}_6\text{S}/\text{C}_4\text{S}-\text{Au}$. As expected, the peak currents exhibit a linear dependence on the scan rate in the range from 0.05 to 0.6 V/s, indicating that the electrode process is characteristic of a surface-confined electroactive layer. The integration of the anodic peak, with correction for the charging current contribution, yields the charge associated with the ferrocene

oxidation Q_{Fc} . This value is used to calculate the surface coverage of the ferrocene Γ from the following relation:

$$\Gamma_{\text{Fc}} = Q_{\text{Fc}}/nFA \quad (14)$$

where n is the number of electrons involved in the electron transfer process ($n = 1$ for ferrocene/ferrocenium), F is the Faraday constant, and A is the geometric surface area of the electrode. The average coverage of ferrocene units is approximately $10^{-10} \text{ mol/cm}^2$ for the two SAMs (see Experimental Section). This value corresponds to about 20% of the theoretical maximum value ($4.5 \times 10^{-10} \text{ mol/cm}^2$) based on the assumption of hexagonal packing of the ferrocene moiety and by treating ferrocene as a sphere of diameter 6.6 \AA .⁵⁰

Since our perturbation process consists of changing the charge of only one ferrocene moiety from 0 to 1, the corresponding ferrocene surface coverage is slightly lower in molecular simulation ($\chi_{\text{Fc}}^{\text{Sur}} = 0.05$) than in electrochemical experiments ($\chi_{\text{Fc}}^{\text{Sur}} = 0.2$). Nevertheless, we have checked that the positions of all atoms of chains along the z -direction exhibit the same behavior at these two low grafting densities (Figure 5). Then, we may conclude that the structural properties of the monolayers are independent of the surface coverage for $\chi_{\text{Fc}}^{\text{Sur}} < 0.2$. In fact, when the mole fraction of Fc is small, the remaining portion of the SAM is thus made up of nonreactive alkylthiolates. So, one can reasonably assume that Fc groups are only in “isolated” states.^{24,51} The presence of an additional peak in the voltammogram assigned to Fc groups in a “clustered” state is obtained from $\chi_{\text{Fc}}^{\text{Sur}} > 0.4$.^{24,51}

For each monolayer, a redox wave due to the one-electron oxidation process ($\text{Fc} \rightarrow \text{Fc}^+$) is obtained (Figure 4) with peak positions that are within the ranges of the redox potentials of ferrocene SAMs reported previously.¹⁴ More precisely, the peak potentials are found to be nearly similar for both ferrocenylalkanethiolate chain lengths (0.25 V/SCE). These experimental results perfectly corroborate the small difference in $\Delta\Delta G_{\text{redox}}^{\text{cal}}$ obtained from perturbation methods. Thus, we establish that the methodology performs very well even in the case of small free energy change. The ability of the different potential models used here to accurately model the energy properties of these SAMs give confidence in the prediction of their structural properties.

We now focus on the microscopic description of these monolayers upon oxidation for deeper interpretation of the thermodynamic trend. We begin the discussion by representing in Figure 6 the molecular density profiles of FcC_6S ferrocenylhexanethiol chain, of coadsorbed C_4S , butanethiol chains, and ClO_4^- counterions. These molecular density profiles are perfectly coincident with those of previous work.²⁷ Briefly, a close examination of Figure 6 reveals that increasing the length of the chains in the ferrocene-terminated thiol does not drastically affect the monolayer thickness. From these profiles, the monolayer thickness of B could be estimated at about 1.5 nm (Figure 6b). This value is smaller than the calculated one expected (1.9 nm) from the thickness of a $\text{C}_{11}-\text{SH}$ ^{53–55} (1.2 nm) and the diameter of a ferrocene group (0.66 nm).⁸ This indicates the tendency of $\text{FcC}_{11}\text{S}/\text{C}_4\text{S}-\text{Au}$ film to deviate from well-arranged structures at low surface mole fractions. We can also observe in Figure 6b a large overlap between the density profiles of FcC_{11} and perchlorate anions. This highlights that the perchlorate anions interact further with the ferricinium cation. Indeed, the energy contribution of this ion pair is about -40 kJ/mol , and the average distance between the two ions is 5.1 \AA .

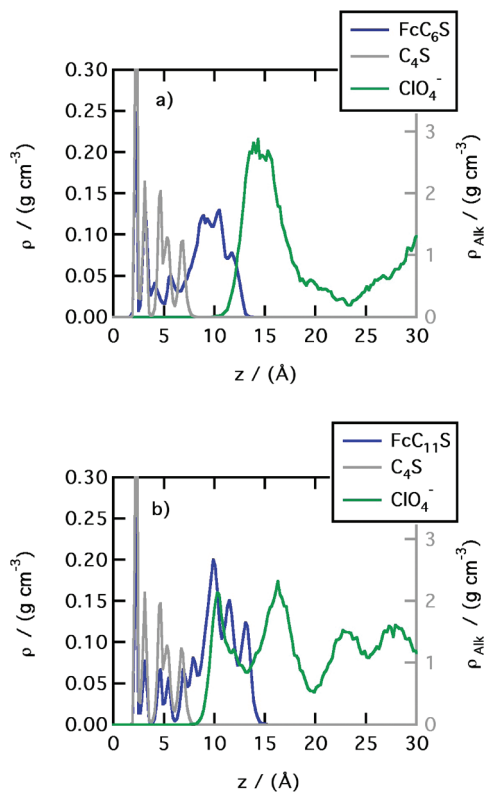


Figure 6. (a) Molecular density profiles of the coadsorbed butanethiolate chains, ferrocenylhexanethiolate chain, and counterions for $\lambda = 1.0$ at $\chi_{\text{Fc}}^{\text{Sur}} = 0.05$. The same profiles are given in panel b where the ferrocenylundecanethiolate chain replaces the ferrocenylhexanethiolate chain.

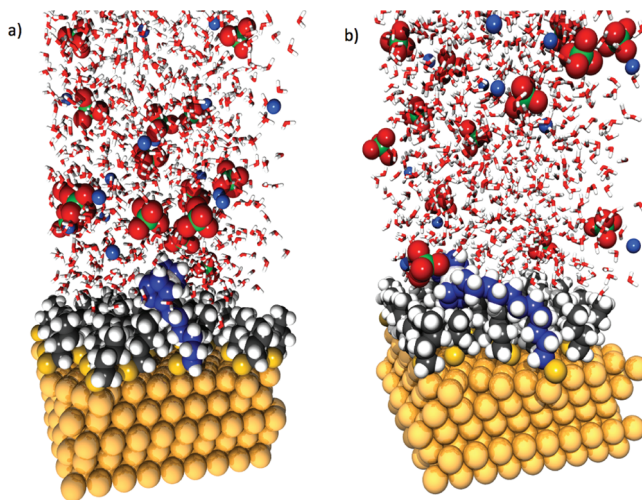


Figure 7. Snapshots of the MD configuration at the monolayer/solution interface at $\chi_{\text{Fc}}^{\text{Sur}} = 0.05$. (a) $\text{FcC}_6\text{S}/\text{C}_4\text{S}-\text{Au}$, (b) $\text{FcC}_{11}\text{S}/\text{C}_4\text{S}-\text{Au}$.

Interestingly, the overlap between the density profiles is less pronounced in A, demonstrating that the formation of ion pair is less favored in this SAM (Figure 6a). As a result, the energy contribution is less favorable (-16 kJ/mol with an average distance of 6.8 \AA). Briefly, the ion pair is stronger in B than in A. A typical configuration of the tight complexation of ClO_4^- by the SAM-bound ferrocenium in B is shown for illustration in

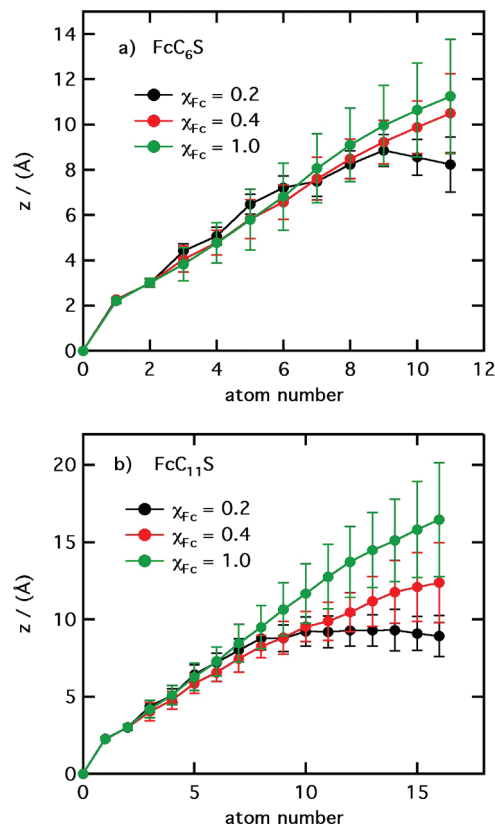


Figure 8. z position of all atoms of the ferrocenylalkylthiolate chains along the z -direction as a function of the surface coverage (see Figure 1 for the atom numbering): (a) $\text{FcC}_6\text{S}/\text{C}_4\text{S}-\text{Au}$; (b) $\text{FcC}_{11}\text{S}/\text{C}_4\text{S}-\text{Au}$.

panel b of Figure 7. In panel a, we have also reported a typical configuration of A.

The thermodynamic cost to be paid for the ion-pair formation is a partial desolvation of anions. A stronger desolvation of the first hydration shell of the perchlorate anion with a loss of 10 water molecules with respect to the bulk occurred in B (against a loss of only two water molecules in A). The contribution ($B - A$) change is enthalpically unfavored $-\Delta H_{\text{redox}}^{\text{calc}} > 0$ and entropically favored $-\Delta S_{\text{redox}}^{\text{calc}} > 0$ (Table 2). The positive enthalpy and entropy changes indicate that the major contribution comes from the partial desolvation of the perchlorate anions upon interaction and from the consequent release of water molecules.

To further analyze the possible low degree of order of $\text{FcC}_{11}\text{S}/\text{C}_4\text{S}-\text{Au}$, the positions of the atoms of ferrocenylalkylthiolate chains are reported for both A and B systems along the z -direction in Figure 8. We examine these positions as a function of the surface coverage before the oxidation of the ferrocene. Interestingly, at $\chi_{\text{Fc}}^{\text{Sur}} = 0.2$ we observe that the average distance of the ferrocene heads with respect to the surface normal is quasi similar for both FcC_{11}S and FcC_6S . Additionally, the z -positions of the last atoms do not change with z in B. This is in perfect agreement with the back folding of the ferrocene moieties in B. The tilting of the terminal part of the chains probably results from the hydrophobic character of the ferrocene headgroup. Obviously, hydrophobic Fc groups prefer to interact with the methyl alkyl chains of the diluent coadsorbate rather than with the hydrophilic interfacial region. This tendency is highly pronounced in B because of the large difference between the two chains' length of the two constituents of the monolayer.

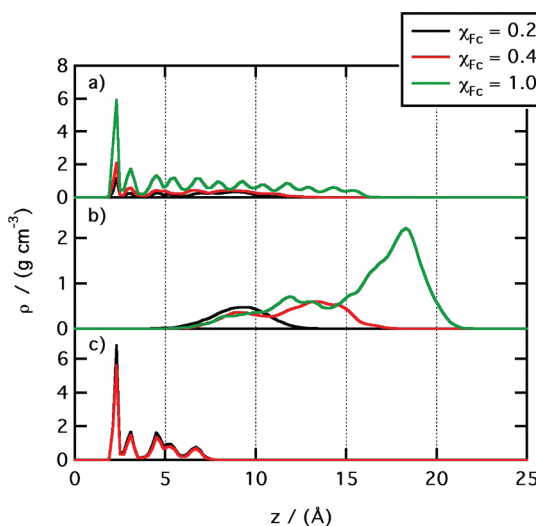


Figure 9. Atomic density profiles of different groups of B along the z -direction, for (a) the alkyl groups of the FcC_{11}S chains; (b) the Fc groups; (c) the diluent coadsorbate C_4S chains.

The propensity of the ferrocene moiety to back folding in the monolayer is well-illustrated in Figure 7. This leads to similar environments of the ferrocene moiety in A and B. This effect is postulated to be partially responsible to the no shift in formal potential (Figure 4) as a function of the chain length of the electroactive component observed at low surface coverage. Finally, it is also interesting to note that the average z -positions of atoms of the second part of the chains (from carbon C8) depend on the surface coverage in B (Figure 8b). It can be noted that, for $\chi_{\text{Fc}}^{\text{Sur}} = 1$, the positions are linearly distributed along z . On the contrary, at lower surface coverage ($\chi_{\text{Fc}}^{\text{Sur}} = 0.2$) the z -positions of the atoms from carbon C8 do not change with z . The increasing average distance of the ferrocene heads with the surface coverage gives rise to a change of the environment around the Fc groups. Additionally, the tilting of the Fc moiety with respect to the surface normal is decreasing from 97° to 63° as the surface coverage is increasing from 0.2 to 1.0. As a result, the ferrocene adopts the more perpendicular orientation at $\chi_{\text{Fc}}^{\text{Sur}} = 1.0$ arising from the steric crowding of the relatively large ferrocene groups. We also examine the effect of the surface coverage for FcC_6S showing that the surface coverage impacts much less on the z -positions of the end groups (Figure 8a).

Figure 9 displays the molecular density profiles of the carbon groups of various groups of the $\text{FcC}_{11}\text{S}/\text{C}_4\text{S}-\text{Au}$ monolayer as a function of the surface mole fraction of Fc along the direction normal to the surface. More precisely, we have reported the molecular density profiles of the FcC_{11}S alkyl chains (Figure 9a), of the Fc groups (Figure 9b) and of the diluent coadsorbate chains C_4S (Figure 9c). At $\chi_{\text{Fc}}^{\text{Sur}} = 0.2$, we observe domains where the three profiles overlap. In perfect agreement with that discussed above, this shows that the Fc chains can penetrate into the monolayer at low surface coverage and introduce a molecular disorder within the monolayer. Figure 9b also reveals that the profile of the Fc groups become more extended with increasing surface coverage. At $\chi_{\text{Fc}}^{\text{Sur}} = 0.4$, the profile becomes even almost uniform. This suggests that the Fc groups sample additional regions in the monolayer compared to $\chi_{\text{Fc}}^{\text{Sur}} = 0.2$. This leads to additional orientational configurations and microenvironments of the ferrocene moiety. These different

Table 3. Energy Contributions (kJ/mol) Involving the Fc Groups in the $\text{FcC}_{11}\text{S}/\text{C}_4\text{S}-\text{Au}$ Film as a Function of the Surface Coverage

contribution	$\chi_{\text{Fc}}^{\text{Sur}} = 0.2$	$\chi_{\text{Fc}}^{\text{Sur}} = 0.4$	$\chi_{\text{Fc}}^{\text{Sur}} = 1$
$E_{\text{Fc}-\text{Fc}}$	-6.8	-26.8	-50.6
$E_{\text{Fc}-\text{Alk}}$	-40.4	-32.5	-29.1
$E_{\text{Fc}-\text{H}_2\text{O}}$	-47.2	-21.5	-13.7
$E_{\text{Fc}-\text{ClO}_4^-}$	-0.01	-2.2	-1.6
$E_{\text{Fc}-\text{Na}^+}$	-0.2	0.2	0.3

microenvironments induce specific macroscopic phenomena, such as the broadening of peaks obtained in electrochemical measurements. They are at the origin of the nonideal electrochemical behavior at relatively high surface coverage of ferrocenylalkylthiolates, as mentioned in the literature.^{52,56–61} For this reason, the majority of researchers employs lower surface coverage to obtain ideal behavior of the ferrocenylalkylthiolate system.

Finally, it is also possible to access of the energetic properties of B from the MD simulations. The formation of self-assembled monolayers depends on the competition among several forces, such as the intrachain, interchain, chain–surface, and chain–bulk interactions, which ultimately determine the molecular orientation near the surface. We are only interested to compare the energy of the interactions involving the ferrocene group as a function of the surface coverage before the oxidation of Fc. In fact, in a previous work, we have demonstrated that these contributions become very similar after the oxidation of Fc into Fc^+ , whereas initially they are quite unlike.²⁷ The total interaction energy of the ferrocene groups has been split into five distinct parts: the interactions with other ferrocene groups ($E_{\text{Fc}-\text{Fc}}$), with alkyl groups ($E_{\text{Fc}-\text{Alk}}$), with water molecules ($E_{\text{Fc}-\text{H}_2\text{O}}$), with perchlorate anions ($E_{\text{Fc}-\text{ClO}_4^-}$), and with sodium cations ($E_{\text{Fc}-\text{Na}^+}$). Each energy contribution sums the Lennard–Jones and electrostatic energy parts. The average contributions obtained are reported in Table 3. Since the separation is large between the ferrocene units at $\chi_{\text{Fc}}^{\text{Sur}} = 0.2$, the contribution of $E_{\text{Fc}-\text{Fc}}$ in the total energy is weak. By contrast, at $\chi_{\text{Fc}}^{\text{Sur}} = 1.0$, the vertical position due in part to smaller distances between the grafting sites of the ferrocene headgroup favors this Fc–Fc interaction. In $\chi_{\text{Fc}}^{\text{Sur}} = 0.2$ the ferrocene groups prefer to interact with the methyl alkyl chains rather than with the hydrophilic interfacial region. Consequently, the lower $\chi_{\text{Fc}}^{\text{Sur}}$ is, the higher $E_{\text{Fc}-\text{Alk}}$ is. Concerning the contribution of $E_{\text{Fc}-\text{H}_2\text{O}}$, it is smaller at $\chi_{\text{Fc}}^{\text{Sur}} = 1.0$ due to the vertical orientation adopted by the chains that favors the Fc–Fc contributions. As expected, the interactions with the supporting electrolyte are negligible in the neutral systems. All of the energy contributions confirm the features discussed here.

CONCLUSION

The free energy perturbation methods were applied to predict the change in the redox potential as the ferrocenylalkanethiolate chain length increased from 6 to 11 carbons. Calculations of enthalpy and entropy differences using molecular simulations were also performed. In fact, our results indicate no significant shift in the redox potential under the conditions used here. The excellent agreement between the simulated and the experimental redox properties establishes that the free energy perturbation methods perform very well even in the case of small free energy

change. This gives confidence in the use of these potentials for the prediction of energy and structural properties of the SAMs.

From the investigation of the microscopic description of these monolayers at low surface coverage, the possibility for the ferrocene moieties in $\text{FcC}_{11}\text{S}-\text{Au}$ to back folding in the monolayer at low surface coverage is established. This leads to similar environments of the ferrocene moiety in A and B. This effect is postulated to be partially responsible to the unchanged formal potential for the surface redox reaction.

In addition, MD simulations show that the ion pair between the one-electron-oxidized ferrocenyl moiety and the electrolyte anion is stronger in B than in A. However, the ion-pair formation is accompanied by a stronger desolvation of the first hydration shell of the perchlorate anions in B (with a loss of 10 water molecules). The fact that the contribution (B – A) change is enthalpically unfavored $-\Delta\Delta H_{\text{redox}}^{\text{calc}} > 0$ and entropically favored $-\Delta\Delta S_{\text{redox}}^{\text{calc}} > 0$ indicates that the major contribution comes from the partial desolvation of the perchlorate anions upon interaction and from the consequent release of water molecules.

The molecular density profiles of the carbon groups of $\text{FcC}_{11}\text{S}-\text{Au}$ alkyl chains, of the Fc groups, and of the coadsorbate $\text{C}_4\text{S}-\text{Au}$ are also reported as a function of the surface coverage in Fc. At low $\chi_{\text{Fc}}^{\text{Sur}}$, the domains where the three profiles overlap are highlighted. Such results can be easily explained by the possibility for the Fc chains to penetrate into the monolayer. At $\chi_{\text{Fc}}^{\text{Sur}} = 0.4$ the profile of the Fc groups becomes almost uniform, showing additional orientational configurations and microenvironments of the ferrocene moiety.

AUTHOR INFORMATION

Corresponding Author

*E-mail: christine.bonal@univ-bpclermont.fr.

ACKNOWLEDGMENT

This work was granted access to the HPC resources of IDRIS under the allocation 2009-i2009092119 made by GENCI (Grand Equipment National de Calcul Intensif). Dr. Isabelle Ripoche is gratefully thanked for the purification of products.

REFERENCES

- (1) Izumi, R.; Hayama, K.; Hayashi, K.; Toko, K. *Chem. Sens.* **2004**, *20*, 50.
- (2) Kishimoto, M.; Ikenaga, Y.; Siigi, H.; Nagaoka, T. *Chem. Sens.* **2002**, *18*, 31.
- (3) Kim, D.-S.; Park, H.-J.; Park, J.-E.; Shin, J.-K.; Kang, S.-W.; Seo, H.-I.; Lim, G. *Sens. Mater.* **2005**, *17*, 259.
- (4) Campuzano, S.; Pedrero, M.; Pingarron, J. *Talanta* **2005**, *66*, 1310.
- (5) Kitagawa, K.; Morita, T.; Kimura, S. *Langmuir* **2005**, *21*, 10624.
- (6) Chen, J.; Reed, M. A.; Rawlett, A. M.; Tour, J. M. *Science* **1999**, *286*, 1550.
- (7) Andres, R. P.; Bein, T.; Dorogi, M.; Feng, S.; Henderson, J. I.; Kubiak, C. P.; Mahoney, W.; Osifchin, R. G.; Reifenberger, R. *Science* **1996**, *272*, 1323.
- (8) Chidsey, C. E. D.; Bertozzi, C. R.; Putwinski, T. M.; Muisce, A. M. *J. Am. Chem. Soc.* **1990**, *112*, 4301.
- (9) Creager, S. E.; Rowe, G. K. *Anal. Chim. Acta* **1991**, *246*, 233.
- (10) Chidsey, C. E. D. *Science* **1991**, *251*, 919.
- (11) Collard, D. M.; Fox, M. A. *Langmuir* **1991**, *7*, 1192.
- (12) Buttry, D. *Langmuir* **1990**, *6*, 1319.
- (13) Ju, H. X.; Leech, D. *Phys. Chem. Chem. Phys.* **1999**, *1*, 1549.
- (14) Rowe, G. K.; Creager, S. E. *Langmuir* **1991**, *7*, 2307.
- (15) Shimazu, K.; Yagi, I.; Sato, Y.; Uosaki, K. *Langmuir* **1992**, *8*, 1385.
- (16) Shimazu, K.; Yagi, I.; Sato, Y.; Uosaki, K. *J. Electroanal. Chem.* **1994**, *372*, 117.
- (17) Sato, Y.; Frey, B. L.; Corn, R. M.; Uosaki, K. *Bull. Chem. Soc. Jpn.* **1994**, *67*, 21.
- (18) Sabapathy, R. C.; Bhattacharyya, S.; Leavy, M. C.; Cleland, W. E. J.; Hussey, C. L. *Langmuir* **1998**, *14*, 124.
- (19) He, Z.; Bhattacharyya, S.; Leavy, M. C.; W. E. Cleland, J.; Hussey, C. L. *Electroanal. Chem.* **1995**, *397*, 305.
- (20) Kondo, T.; Horiuchi, S.; Yagi, I.; Ye, S.; Uosaki, K. *J. Am. Chem. Soc.* **1999**, *121*, 391.
- (21) Popenoe, D.; Deinhammer, R. S.; Porter, M. D. *Langmuir* **1992**, *8*, 3157.
- (22) Ye, S.; Sato, Y.; Uosaki, K. *Langmuir* **1997**, *13*, 3157.
- (23) Ye, S.; Sato, T. H. Y.; Shimazu, K.; Uosaki, K. *Phys. Chem. Chem. Phys.* **1999**, *1*, 3653.
- (24) Goujon, F.; Bonal, C.; Limoges, B.; Malfreyt, P. *Langmuir* **2009**, *25*, 9164.
- (25) Goujon, F.; Bonal, C.; Malfreyt, P. *Mol. Simul.* **2009**, *35*, 538.
- (26) Goujon, F.; Bonal, C.; Limoges, B.; Malfreyt, P. *J. Phys. Chem. B* **2008**, *112*, 14221.
- (27) Goujon, F.; Bonal, C.; Limoges, B.; Malfreyt, P. *J. Phys. Chem. B* **2010**, *114*, 6447.
- (28) Filippini, G.; Goujon, F.; Bonal, C.; Malfreyt, P. *J. Phys. Chem. B* **2010**, *114*, 12897.
- (29) Cornell, W. D.; Cieplak, P.; Bayly, C. I.; Gould, I. R.; Merz, K. J.; Ferguson, D. M.; Spellmeyer, D. M.; Fox, T.; Caldwell, J. W.; Kollman, P. *J. Am. Chem. Soc.* **1995**, *117*, 5179.
- (30) Rai, B.; Sathish, P.; Malhotra, C. P.; Pradip; Ayappa, K. G. *Langmuir* **2004**, *20*, 3138.
- (31) Lopes, J. N. C.; do Couto, P. C.; da Piedade, M. E. M. *J. Phys. Chem. A* **2006**, *110*, 13850.
- (32) Ryckaert, J. P.; Cicotti, G.; Berendsen, H. J. C. *J. Comput. Phys.* **1977**, *23*, 327.
- (33) Abascal, J. L. F.; Vega, C. *J. Chem. Phys.* **2005**, *123*, 234505.
- (34) Goujon, F.; Bonal, C.; Limoges, B.; Malfreyt, P. *Mol. Phys.* **2008**, *106*, 1397.
- (35) Klähn, M.; Seduraman, A.; Wu, P. *J. Phys. Chem. B* **2008**, *112*, 10989.
- (36) Essmann, U.; Perera, L.; Berkowitch, M. L.; Darden, T.; Lee, H.; Pedersen, L. G. *J. Chem. Phys.* **1995**, *98*, 103, 8577.
- (37) Fuchs, K. *Proc. R. Soc. A* **1935**, *151*, 585.
- (38) Yeh, I.-C.; Berkowitz, M. L. *J. Chem. Phys.* **1999**, *111*, 3155.
- (39) Smith, E. R. *Proc. R. Soc. London, Ser. A* **1981**, *375*, 475.
- (40) Ghoufi, A.; Malfreyt, P. *Mol. Phys.* **2006**, *104*, 2929.
- (41) DL-POLY is a parallel molecular dynamics simulation package developed at the Daresbury Laboratory Project for Computer Simulations under the auspices of the EPSRC for the Collaborative Computational Project for Computer Simulation of Condensed Phases (CCPS) and the Advanced Research Computing Group (ARCG) at the Daresbury Laboratory.
- (42) Hoover, W. G. *Phys. Rev. A* **1985**, *31*, 1695.
- (43) Honenberg, P.; Kohn, W. *Phys. Rev. A* **1964**, *136*, 864.
- (44) Kohn, W.; Sham, L. *J. Phys. Rev. A* **1965**, *140*, 1133.
- (45) Becke, A. D. *Phys. Rev. A* **1988**, *38*, 3098.
- (46) Becke, A. D. *J. Chem. Phys.* **1993**, *98*, 5648.
- (47) Perdew, J. P.; Wang, Y. *Phys. Rev. E* **1991**, *45*, 13244.
- (48) Frisch, M. J., et al. Gaussian, Inc.: Wallingford, CT, 2004.
- (49) Breneman, C. P.; Wiberg, K. B. *J. Comput. Chem.* **1990**, *11*, 361.
- (50) Seiler, P.; Dunitz, J. D. *Acta Crystallogr.* **1979**, *B35*, 1068.
- (51) Lee, L. Y. S.; Sutherland, T. C.; Rucaleanu, S.; Lennox, R. B. *Langmuir* **2006**, *22*, 4438.
- (52) Rowe, G. K.; Creager, S. E. *J. Phys. Chem.* **1994**, *98*, 5500.
- (53) Bain, C. D.; Troughton, E. B.; Tao, Y. T.; Evall, J.; Whitesides, G. M.; Nuzzo, R. G. *J. Am. Chem. Soc.* **1989**, *111*, 321.
- (54) Biebuyk, H. A.; Bain, C. D.; Whitesides, G. M. *Langmuir* **1994**, *10*, 1825.

- (55) Porter, M. D.; Bright, T. B.; Allara, D. L.; Chidsey, C. E. D. *J. Am. Chem. Soc.* **1987**, *109*, 3559.
- (56) Chambers, R. C.; Inman, C. E.; Hutchison, J. E. *Langmuir* **2005**, *21*, 4615.
- (57) Voicu, R.; Ellis, T. H.; Ju, H.; Leech, D. *Langmuir* **1999**, *15*, 8170.
- (58) Rowe, G. K.; Creager, S. E. *Langmuir* **1994**, *10*, 1186.
- (59) Seo, K.; Jeon, I. C.; Yoo, D. J. *Langmuir* **2004**, *20*, 4147.
- (60) Kawaguchi, T.; Tada, K.; Shimazu, K. *J. Electroanal. Chem.* **2003**, *543*, 41.
- (61) Auletta, T.; van Veggel, F. C. J. M.; Reinhoudt, D. N. *Langmuir* **2002**, *18*, 1288.